

Measurement of the directional sensitivity of DMTPC detectors

Cosmin Deaconu,^{1,*} Michael Leyton,^{1,†} Ross Corliss,¹ Gabriela Druitt,² Richard Eggleston,² Natalia Guerrero,^{2,‡} Shawn Henderson,^{1,§} Jeremy Lopez,^{1,¶} Jocelyn Monroe,² and Peter Fisher³

¹*Physics Department, and Laboratory for Nuclear Science, Massachusetts Institute of Technology, 77 Massachusetts Avenue, Cambridge, Massachusetts 02139*

²*Royal Holloway University of London, Department of Physics, Egham, Surrey TW20 0EX, United Kingdom*

³*Physics Department, Institute for Soldier Nanotechnology, MIT Kavli Institute and, Laboratory for Nuclear Science, Massachusetts Institute of Technology, 77 Massachusetts Avenue, Cambridge, Massachusetts 02139***

(Dated: September 11, 2018)

The Dark Matter Time Projection Chamber (DMTPC) is a direction-sensitive detector designed to measure the direction of recoiling ^{19}F and ^{12}C nuclei in low-pressure CF_4 gas using optical and charge readout systems. In this paper, we employ measurements from two DMTPC detectors, with operating pressures of 30–60 torr, to develop and validate a model of the directional response and performance of such detectors as a function of recoil energy. Using our model as a benchmark, we formulate the necessary specifications for a scalable directional detector with sensitivity comparable to that of current-generation counting (non-directional) experiments, which measure only recoil energy. Assuming the performance of existing DMTPC detectors, as well as current limits on the spin-dependent WIMP-nucleus cross section, we find that a 10–20 kg scale direction-sensitive detector is capable of correlating the measured direction of nuclear recoils with the predicted direction of incident dark matter particles and providing decisive (3σ) confirmation that a candidate signal from a non-directional experiment was indeed induced by elastic scattering of dark matter particles off of target nuclei.

I. INTRODUCTION

The nature of dark matter presents the major challenge to the current theory of particle interactions. Weakly Interacting Massive Particles (WIMPs), motivated by supersymmetry and other theories with new physics at the 100 GeV energy scale, provide an important candidate for dark matter. For thirty years, counting experiments have sought detection of nuclear recoils induced by the elastic scattering of neutral particles with 10–1,000 GeV/ c^2 mass and $\beta \sim 0.001$, improving the cross section sensitivity from that of a very massive Dirac neutrino, 10^{-34} cm^2 , to the current limit of 10^{-45} cm^2 .

In the event of a statistically significant observation by a counting experiment measuring only the recoil energy spectrum, confirmation that the observed events resulted from the elastic scattering of dark matter particles off of target nuclei will be crucial. While measurement with other target isotopes may give some comfort that a candidate signal was caused by dark matter, correlation with an astrophysical phenomenon will be essential. The mo-

tion of the Solar System through the galactic dark matter halo provides two means of establishing an astrophysical correlation: the annual modulation of the count rate above a threshold energy and the sidereal variation in the recoil direction of a struck target nucleus. Discussions surrounding the claimed observations of annual modulation of the recoil rate have shown that this method may be prone to instrumental and environmental systematics [1]; we have therefore pursued the more difficult, but more decisive, sidereal directional modulation technique.

The recoil energy spectrum of nuclei struck by WIMPs falls exponentially with energy with an e -folding factor proportional to the average WIMP kinetic energy. The maximum nuclear recoil energy ranges from 5 to 250 keV, depending on WIMP and target nucleus masses. Nuclear recoil experiments therefore place a premium on low energy thresholds. A fluorine recoil with 40 keV energy in 60 torr of CF_4 gas will have a typical track length of $\mathcal{O}(1 \text{ mm})$. Reconstructing the direction of such a recoil requires a detector with spatial resolution of 300 μm (or higher) to measure at least three points along the track. At this pressure, probing meaningful cross-sections requires detectors with tens or hundreds of cubic meters of target volume [2].

We have carried out a performance study of a 20-liter DMTPC detector [3], scalable to a cubic meter, to understand whether loss of directional information occurs due to physics processes, instrumentation, or both. Our measurements support a model that allows us to assess the directional performance of a cubic-meter DMTPC detector that we have built and are currently commissioning [4]. We show that an array of cubic meter detectors could confirm or refute a claimed observation by

*Currently at the Kavli Institute for Cosmological Physics, University of Chicago, Chicago, Illinois 60637

†Currently at Institute of High-Energy Physics, Barcelona Institute of Science and Technology, 08193 Bellaterra, Spain

‡Currently at MIT Kavli Institute, 77 Massachusetts Ave. Cambridge MA 02139

§Currently at Cornell University, Department of Physics, Ithaca, New York 14853

¶Currently at Department of Physics, University of Colorado at Boulder, Boulder CO 80309

**Corresponding author: fisherp@mit.edu

the current generation of counting experiments for spin-dependent interactions. (Due to the nuclear structure of ^{19}F , DMTPC detectors are primarily sensitive to spin-dependent WIMP coupling.) We use our measurements to provide, for the first time, a quantitative baseline for evaluating the detection technology of direction-sensitive searches, and to identify places for improvement in the directional technique.

II. DETECTOR DESCRIPTION

Time projection chambers (TPCs) [5] achieve better than $100\text{-}\mu\text{m}$ spatial resolution in the drift direction over large sensitive volumes. By using drift lengths of up to several meters to transport ionization electrons from the site of a recoil event to an amplification and readout plane, TPCs achieve high spatial resolution for large sensitive volumes, at a low channel count. Proportional amplification gives two-dimensional information on the recoil direction in the plane perpendicular to the drift. The optical readout system in DMTPC images the amplification plane and measures scintillation light produced during proportional amplification, thereby measuring a two-dimensional projection of the recoil onto the readout plane. Transient charge readout of the anode gives information about the ionization distribution along the drift direction, i.e. the axis normal to the amplification plane. Photomultiplier tubes (PMTs) measure the total light output with nanosecond time resolution and give information about the recoil along the drift coordinate direction.

In this paper, we model the performance of a 20-liter TPC with optical and charge readout systems, referred to as the 4Shooter [3]. The cylindrical drift volume of the 4Shooter detector is housed within a set of field-shaping rings and measures 30.7 cm in diameter and 26.7 cm from cathode to anode, resulting in a sensitive volume of 19.8 liters of CF_4 at 30–100 torr and a target mass of 2–10 g. The ground mesh is 80% transparent and stands $435\ \mu\text{m}$ above the anode plane. For the measurements presented here, the anode was held at 670 V, creating an electric field of 15 kV/cm and a measured gas gain of 67,000, calibrated using an ^{55}Fe X-ray source. Typical drift fields were 180–200 V/cm, chosen to minimize the diffusion of the electron swarm during the drift.

The optical system ($4 \times$ Canon 85 mm $f/1.2$ lenses, with a magnification of 6.67, mounted onto $4 \times$ Apogee Alta U6 CCD cameras with Kodak KAF-1001E chips) has a geometric acceptance of 7×10^{-4} , on average, per camera and lens, for photons originating from the amplification region. The four CCD cameras collect the scintillation light emitted during proportional multiplication between the grounded mesh and anode plane. More details can be found in Ref. [3]. The cameras were operated in ‘witness’ (continuous) mode, typically imaging for one second before being read out. Transient charge and light signals were collected during each exposure and stored

along with the CCD image. The optical system gain was calibrated using an ^{241}Am α source, depositing approximately 4.0 MeV per α in the sensitive volume and producing 10–19 counts/keV $_{ee}$, depending on the camera [3]. Here, we use the subscript $_{ee}$ to denote electron-equivalent energy since not all of the recoil energy is converted into ionization, particularly for nuclei. Conversion factors between recoil energy and electron-equivalent energy are estimated using TRIM [6]. Nuclear recoils were generated within the detector volume using AmBe and ^{252}Cf neutron sources.

For the measurements presented here, we also used a small chamber with a 10-cm-diameter ‘triple-mesh’ amplification region, consisting of a shared anode mesh sandwiched between two ground meshes, allowing optical readout of two back-to-back TPCs with a single camera. The gas gain measured in this mode was about 100,000. We also operated the triple-mesh amplification region in ‘cascade’ mode, resulting in a maximum achievable gas gain of approximately 10^6 at a gas pressure of 30 torr for a single TPC. However, most of our data with this chamber was collected with a gas gain of 440,000. The optical system consisted of a Nikkor 55 mm $f/1.2$ lens mounted onto an Andor Ikon L936 camera. The optical system gain was estimated to be approximately 300 counts/keV $_{ee}$.

III. DETECTOR RESPONSE

We model the directional response of a DMTPC detector by simulating the steps shown in Fig. 1 and comparing with calibration data collected from our detectors. The sequence of events in the detector starts with the velocity distribution of WIMPs near Earth and ends with the fit parameters of the reconstructed track associated to a nuclear recoil induced by elastic scattering of a WIMP with a ^{12}C or ^{19}F nucleus. In the study reported here, the data input to the track fit is a CCD image of a nuclear recoil and the output is the recoil direction in the amplification plane. This study does not yet include information from the time structure of the charge readout in the track reconstruction, which can also be used to determine the recoil angle in the drift direction. Instead, information from the charge readout system has been used to improve energy resolution and discriminate against backgrounds coming from radioactivity of the internal components or cosmic rays passing through the CCD sensors.

We simulate recoils of ^{19}F or ^{12}C nuclei due to incident WIMPs, neutrons from a deuterium-deuterium ($d-d$) source and neutrons from an AmBe source. For WIMP-induced recoils, we sample velocities from the Standard Halo Model [7] (SHM), which assumes an isotropic, isothermal sphere for the galactic dark matter distribution, and generate elastic recoils using two-body kinematics with isotropic scattering in the rest frame. For AmBe and $d-d$ sources, we sample the neutron energy from the appropriate distribution, given the source location outside of the detector. In both cases, we generate

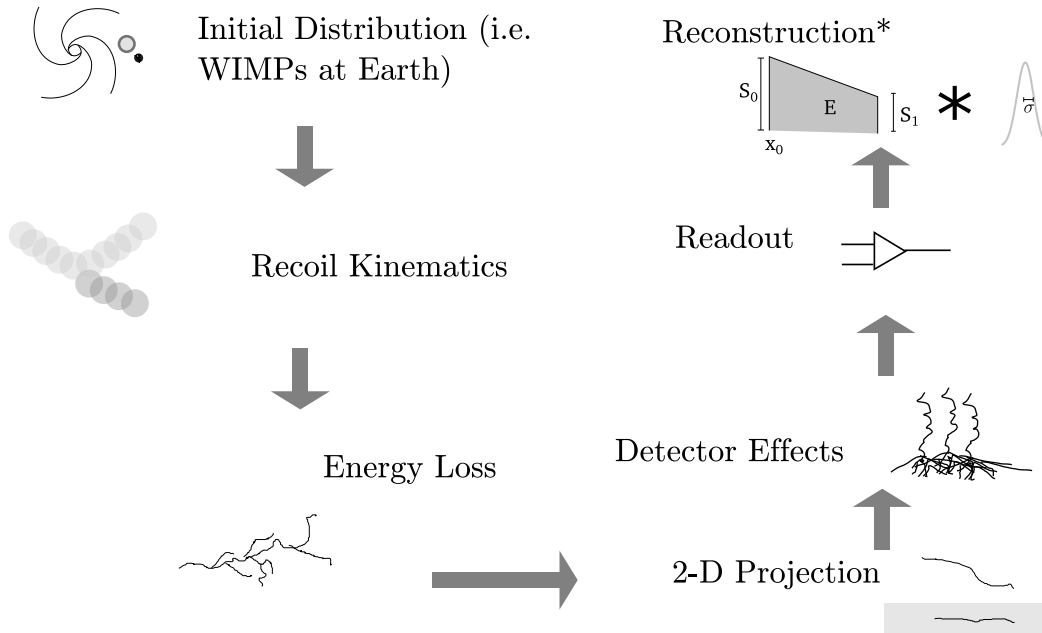


FIG. 1: Flow chart of events depicting the generation, amplification, detection and analysis of WIMP-induced elastic scattering. The * indicates the fit function is a convolution of a linear energy loss with a two dimensional gaussian spatial resolution.

nuclear recoils uniformly throughout the active volume of the detector.

Elastic scattering of WIMPs with masses in the range of 10–1,000 GeV/c^2 off of target nuclei with masses in the range of 10–20 amu impart up to 200 keV of kinetic energy to the recoiling nucleus. Neutrons from AmBe and $d-d$ sources induce nuclear recoils in the same range of energies. We simulate recoiling ^{19}F or ^{12}C nuclei with kinetic energies below 200 keV. In this energy range, recoils lose energy via Coulomb interactions with atomic electrons (electronic stopping), which directly results in ionization, and via screened Coulomb interactions with atomic nuclei (nuclear stopping) [6]. Nuclear stopping, which dominates over electronic stopping below approximately 50 keV for ^{19}F in CF_4 , produces secondary ions that, then, also lose energy, resulting in indirect ionization losses by the primary ion. A single collision can produce energetic secondaries, causing the primary recoiling nucleus to scatter by a large angle, as illustrated in Fig. 2. We use TRIM [6] to simulate the secondary cascades from low-energy ^{19}F ions in low-pressure CF_4 in detail [8]. The trajectories of all recoils in the cascade in TRIM are then used to estimate the three-dimensional ionization distribution resulting from the simulated primary recoil.

DMTPC measures the electrons liberated by the ionization of CF_4 molecules due to the motion of a recoiling ^{19}F or ^{12}C nucleus. The work function of CF_4 is 34 eV/pair [9]. An electric field in the drift volume of $E = 190 \text{ V/cm}$ transports the electrons towards the am-

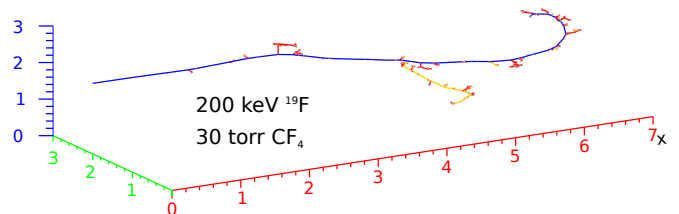


FIG. 2: A TRIM-generated recoil cascade in 30 torr CF_4 . The blue line represents the trajectory of the initial ion, a 200 keV fluorine recoil. The red and yellow lines represent the paths of secondary fluorine and carbon nuclear recoils, respectively. The electron ionization is not shown. The units on the plot are in mm.

plification region with a velocity of $13 \text{ cm}/\mu\text{s}$ [10]; the field strength E is chosen to minimize transverse diffusion. With the 4Shooter detector, we measured the ratio of the electron transverse diffusion constant to the electron mobility, D_T/μ , by parameterizing the transverse track width σ_T as a function of the drift distance, z :

$$\sigma_T^2(z) = \sigma_{T,0}^2 + 2 \left(\frac{D_T}{\mu} \right) \left(\frac{z}{E} \right), \quad (1)$$

where $D_T/\mu = 0.053 \pm 0.005 \text{ V}$ and $\sigma_{T,0} = 0.72 \pm 0.05 \text{ mm}$ are the best fit averages across cameras at a pressure of 60 torr [3]. Our measured value for D_T/μ is consistent with the literature, while the additional $\sigma_{T,0}$ term in-

cludes contributions from various effects such as the intrinsic track width, avalanche width, mesh grid spacing, lens depth-of-focus, and camera resolution. The transverse diffusion is approximately 1 mm for a 25 cm drift distance at 60 torr.

Once at the ground plane, the ionization electrons are guided by the electric field, through the 250- μm -pitch mesh, and into the amplification region. The 15 kV/cm electric field causes proportional multiplication with a net electron gain of up to 10^6 [8]. Scintillation photons are produced during proportional multiplication 34% of the time [11]. These photons image the electron swarm created by the nuclear recoil. We calculate the electric potential in the amplification region due to the woven mesh electrode structure using `gmsht` [12] and `ElmerFEM` [13]. The resulting potential map is then passed to a `garfield++` [14] library to perform the microscopic simulation of the avalanche, recording the spatial distribution of the ionization. For the 4Shooter detector, simulation suggests that the avalanche adds 100 μm to the transverse width of the track. Production of scintillation light is simulated by sampling the ionization distribution and transporting the scintillation photons through the optical viewport and lens to the CCD camera. This step takes view factors and light attenuation of the optics into account. Simulation of the camera response to the incident photons includes the scintillation wavelength spectrum and the CCD quantum efficiency, as well as the measured camera bias and read noise.

A. Readout and Reconstruction

Ref. [8] describes the offline processing of the CCD images and simulated recoils in detail. A brief summary is presented here. In the case of simulated recoils, the camera bias level and read noise from data are added to the simulated images. Images are then cleaned to remove CCD artifacts such as hot pixels, cosmic rays and residual bulk images. Next, dark frames are used to subtract pedestal offsets between pixels and the optical system gain calibration from the ^{241}Am source is applied. Track finding begins by low-pass filtering the image to improve the signal-to-noise ratio for pattern recognition, followed by a custom hysteresis-thresholding segmentation algorithm [8] to build clusters around seed pixels with counts above threshold. Neighboring clusters are merged, particularly when separated by known dead regions of the detector. The clusters are then cleaned of pixels below a minimum threshold. The resulting clusters correspond to the two-dimensional projections of the electron swarms onto the amplification plane. A final classification step identifies the cluster as a spark, residual bulk image, CCD artifact, cosmic ray, α track, or a nuclear recoil inside or outside of the fiducial region. Only the last category of events is used for this directional study. Non-nuclear-recoil events are removed by applying the same set of cuts in data and simulation, described in detail in Ref. [8].

Track parameters from selected clusters associated to nuclear recoils are estimated in the following way for both data and simulation. The intensity values of the pixels comprising the track are modeled as $I(x, y) = G(x, y)S(x, y) + N(x, y)$, where x and y refer to the position on the CCD chip, G is the spatially-dependent system gain (counts/ionization) and S is the best fit of the track ionization density model, averaged over each pixel. N is the predicted number of noise counts in each pixel and is modeled as a combination of Gaussian camera read noise and Poisson shot noise. $S(x, y)$ is the convolution of a Gaussian model of the diffusion and avalanche spreading in the amplification region with a line segment with linearly varying ionization density. We find that this line segment model is a useful approximation to the Bragg curve. Seven parameters fully characterize the track: ionization energy (E_I), one end of the track (x_0, y_0), the track axis (ϕ), the initial ionization density (S_0), the change in ionization density over the length of the track (ΔS), and the convolution width (σ). `Minuit2` [15] carries out the minimization, with initial values based on a principal component analysis of the intensity-weighted pixels belonging to a track.

The angle ϕ gives the reconstructed average axis of ionization of the recoil in the amplification plane and ΔS provides the direction, or sense, along the axis defined by ϕ . For recoil energies below the Bragg peak (~ 1 MeV for fluorine), the ionization profile (dE/dx) decreases with energy. The asymmetry in ionization density along the track direction is used as an estimator of the vector direction. Determining the sign of ΔS presents the key challenge of this work, referred to as the sense or “head-tail” assignment of the track along the axis defined by ϕ . For nuclear recoils below ~ 1 MeV, $\Delta S < 0$ means the ion lost more energy at the start of the track than at the end and that (x_o, y_o) refers to the start of the track, while $\Delta S > 0$ means that (x_o, y_o) refers to the end of the track.

Fig. 3 shows the probability, or efficiency, of correctly assigning the head-tail sense in simulated recoils without consideration of any detector effects. A value of 1.0 on the ordinate of Fig. 3 means that the correct head-tail assignment is always made. Guessing blindly corresponds to a value of 0.5, meaning the guess is correct half of the time. This plot shows that there is considerable loss of information before any detector effects are considered, coming mainly from nuclear collisions during the stopping of the primary recoiling ion in the surrounding gas. We will return to this point later, as this is an important point for the detector performance: the fraction of recoils assigned the correct sense in Fig. 3 shows the maximum possible efficiency. A perfect detector using this direction assignment method would measure a head-tail fraction of 0.7 at a recoil energy of 100 keV.

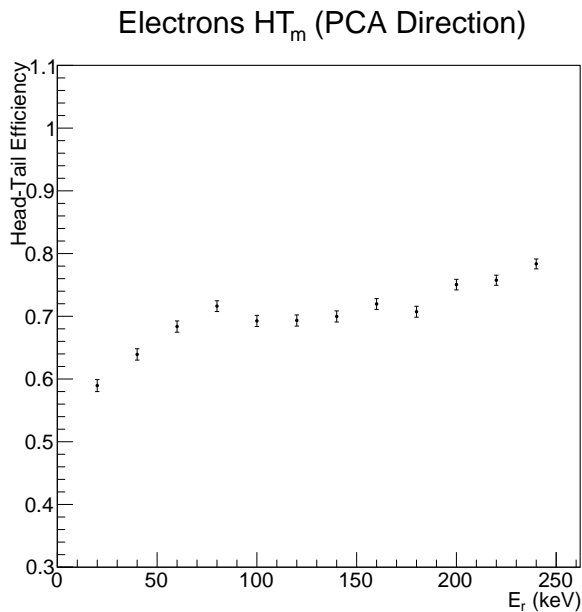


FIG. 3: The simulated fraction of recoils at 30 torr assigned the correct vector sense, or “head-tail”, based on the slope of a line fit, ΔS , to the ionization density deposited onto the CCD chip using a principal component axis, prior to any detector effects.

IV. EXPERIMENTAL MEASUREMENT OF DIRECTIONAL PERFORMANCE

We have carried out three measurements aimed at quantifying the directional performance of DMTPC detectors, namely how well they measure the axis and sense of a recoiling nucleus. This section describes each measurement and compares it with predictions from the simulation.

A. Measurements using α particles

The directional performance is studied using measurements of α particles with known position and direction. We simulate low-energy recoil nuclei by placing a collimated ^{241}Am source above the detector cathode of the 4Shooter detector such that only the last few hundred keV of the α 's enter the fiducial volume. This configuration generates low-energy ^4He tracks at a shallow angle at the maximum drift distance from the anode. While the directional response to low-energy ^4He is not interesting for dark matter searches in pure CF_4 , the simplicity of the setup allows for a well-controlled test of the simulation model. For this measurement the 4Shooter detector was operated at 60 torr, with a gas gain of 67,000.

We measure the gain using ^{55}Fe and ^{241}Am sources mounted inside the vacuum vessel. ^{55}Fe emits photons with energies of 5.9 keV and 6.5 keV that produce electrons in CF_4 gas via photoelectric absorption. ^{55}Am

emits x-rays with energies of 13.9, 17.5, and 21.1 keV [16]. We compared the gas gain measured with Cremat CR-112 and CR-113 charge integrating amplifiers with gains of 13 and 1.3 mV/pC, respectively, and found agreement at the 2% level. Using a work function of 34 eV/pair for CF_4 and carrying out the gain calibration at several pressures gives an additional uncertainty of 5%. Combining data from both ^{55}Fe and ^{241}Am sources gives a calibration linear to within 1.5 [16]. Quenching factors from TRIM [6] are also included, giving results comparable to those measured by the MIMAC collaboration [17], who reported a quenching factor of 0.38 in CF_4 at 50 mbar (37.5 torr) for ^{19}F recoils with 20 keV of energy.

The full detector simulation, adjusted to match the measured system gain, was used to simulate the same scenario. The directional response of both data and simulation are shown in Fig. 4, indicating generally good agreement between the two. Simulation predicts a level of head-tail assignment a few percent better than we find in the data, while the angular spread of recoils is at a similar level as predicted. This gives confidence in the simulation model of the gas physics and recoil response.

B. Measurements using high-energy neutrons

A neutron source is used to study the directional performance with nuclear recoil tracks, similar to a WIMP-induced signal. We used a Troxler Laboratories 3320 AmBe fast neutron source positioned near the 4Shooter detector to produce low-energy ^{19}F and ^{12}C recoils. The detector collected data for 5.4 live days. The source was located several meters from the detector, sufficiently far to ensure a collimated beam of incoming neutrons, but sufficiently close to sustain a relatively high neutron flux. The gain calibration described in the previous section is used for this study.

The AmBe source produces neutrons through an α - n process, where approximately 10^{-4} of the α 's from the ^{241}Am decay produce a neutron via $\alpha + ^9\text{Be} \rightarrow ^{13}\text{C}^* \rightarrow ^{12}\text{C} + n$. The resulting neutron energy spectrum has several peaks and extends up to approximately 12 MeV. Ref. [18] provides a reference spectrum, but the actual spectrum depends on the details of the construction of the source. A two-inch lead-brick shield was placed in front of the neutron beam in order to reduce the rate of sparking in the amplification region induced by the high rate of γ rays from the ^{237}Np decay. We used a Geant4-based [19] simulation to account for the neutron interactions in the lead brick. The resulting neutron energy spectrum is broadly similar to that of Ref. [18], but the simulated spectrum has a larger average recoil angle with respect to the source direction. We simulate events between 40 and 200 keV $_{ee}$ and find that, with a modest track reconstruction fit quality requirement of $\chi^2/n_{\text{dof}} < 2$, the efficiency of reconstructing nuclear recoil tracks in this energy range with the 4Shooter detector is 36%.

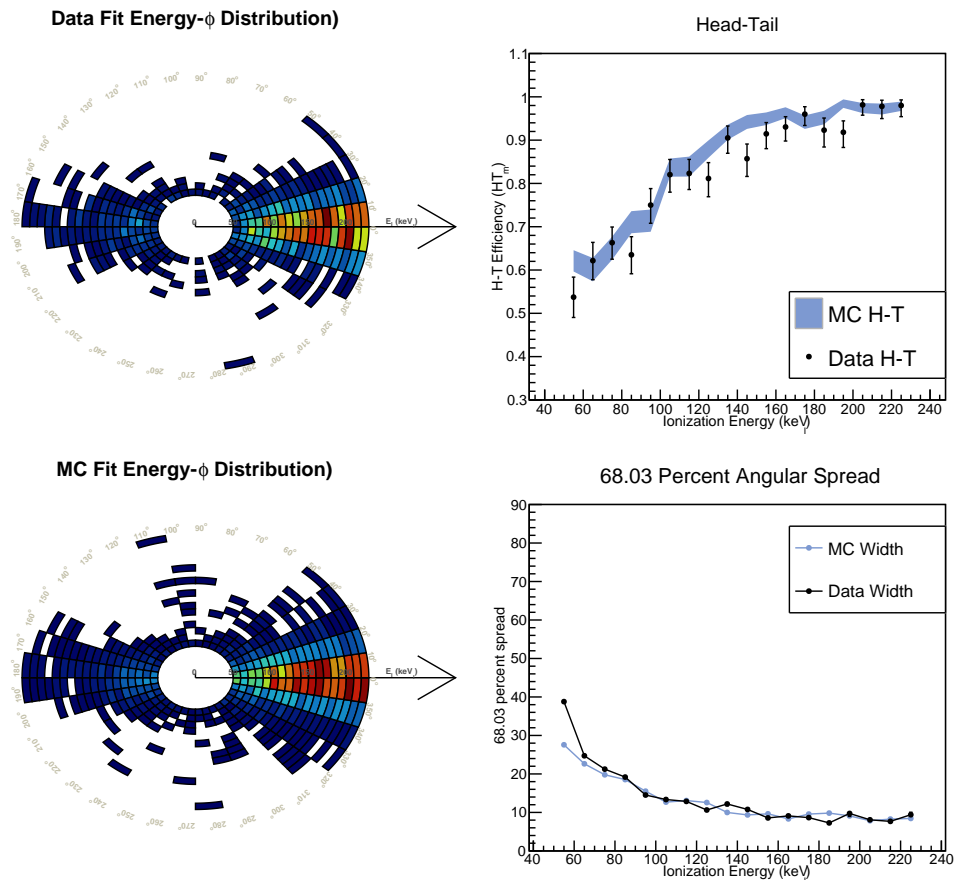


FIG. 4: The directional response to angled α 's for data and simulation. The head-tail efficiency plot shows the fraction of tracks reconstructed with the correct sense, while the axial spread plot shows the angular spread (in $^\circ$) containing 68% of tracks. The colors on the energy- ϕ plots (left) scale linearly from ~ 0 (blue) to a maximum of 0.02 (red).

Fig. 5 shows the energy-angle spectrum measured in data and predicted by the simulation. The angular spread shows 25, 50, and 75% quantiles, since due to kinematics, the peak of the recoil direction spectrum is not expected to be in the mean direction of the neutrons at low energies. The simulated head-tail efficiency is generally in agreement with that measured in data, while the predicted angular spread in direction is 10–20% larger in simulation. This is likely due to uncertainties in the angular distribution of neutrons emitted by the source.

C. Measurements with low-energy neutrons

We studied the directional performance versus lower recoil energies by illuminating the 10-cm test chamber, described in Section II, with a deuterium-deuterium ($d-d$) neutron generator designed by Schlumberger. A $d-d$ neutron generator fuses deuterons via the reaction $d + d \rightarrow {}^3\text{He} + n$, which produces neutrons with an energy of 2.45 MeV and results in nuclear recoils with a maximum possible recoil energy of $\mathcal{O}(500)$ keV. X-ray sources are used to determine the gas gain, as described

above. The location of the Bragg peak at 21 keV/mm for CF_4 at 30 torr [8] serves as a useful cross check with the gain calibration. The general agreement between data and MC for the energy-range recoil distributions shows that the energy scale is linear to within 10% across the range 25 – 500 keV.

In this detector, the nuclear recoil detection efficiency is estimated to be 35% for tracks in the range of 5–200 keV $_{ee}$ by comparing data and simulation, with the same recoil event selection and reconstruction quality cuts as described above. For this study, the high gas gain of the cascaded amplification system caused a small non-Gaussian effect, described in the Appendix in more detail. We accounted for this effect by adding a second Gaussian to the track fit described in Section III A and fitting for the two additional parameters.

Fig. 6 compares the directional response of the detector between data and simulation and shows that the reconstructed range-energy distributions are broadly consistent between the two. Similar to the previous study with AmBe neutrons, the angular spread of the recoil directions predicted by the simulation is larger than that observed in the data, whereas the data contain a larger

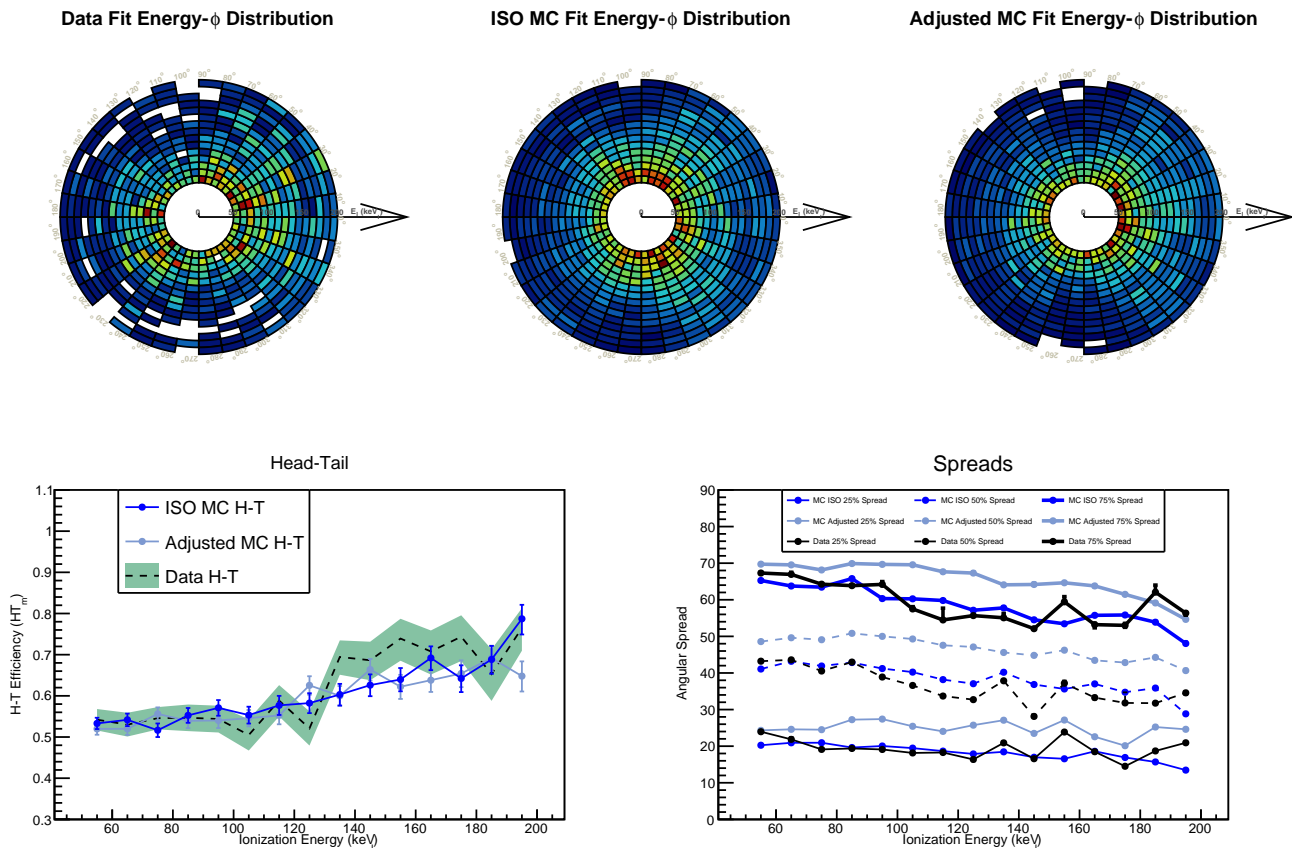


FIG. 5: Measured and simulated energy-angle spectra from the AmBe source. Two different assumptions about the initial neutron spectrum are used, with and without lead shielding, as described in the text. The colors on the energy- ϕ plots (top) scale linearly from ~ 0 (blue) to a maximum of 0.006 (red).

fraction of recoils pointing along the mean direction of the incident neutrons. A likely explanation is that the simulation assumes mono-energetic neutrons, while we calculate that roughly 10% of the neutrons interact in the generator casing or chamber wall before reaching the fiducial volume, which modifies the energy spectrum of incident neutrons. Additional modeling of the neutron propagation may be able to produce better agreement.

Fig. 6 shows good agreement between the head-tail assignment efficiency in simulation and in data, which approaches 70% for recoil energies above 140 keV. By comparison, the maximum measurable head-tail efficiency before any detector effects, shown in Fig. 3, is also 70% at a recoil energy of 140 keV. This is an important benchmark, demonstrating that the DMTPC detector technology discussed here successfully measures the intrinsic directionality of the recoil signal, and that the fundamental physics limit of this approach is the straggling of the primary ^{19}F or ^{12}C ion in the target gas. This property of CF_4 as a target gas is also relevant to other target gases, such as CS_2 , and therefore applicable to all current TPC-based directional experiments.

V. DIRECTIONAL SENSITIVITY

In this section, we develop a metric for quantifying the directional performance of DMTPC detectors using the axial and head-tail measurements of recoiling nuclei discussed in the previous section. We then use this metric to outline the specifications of a directional detector capable of establishing whether a putative signal from a current-generation non-directional, counting experiment has a sidereal variation in direction.

Given the large fluctuations in energy loss at low energies, the performance metric defined here combines both the axial direction reconstruction and the head-tail assignment to utilize all available directional measurement information. We define an opening angle, called the axial spread, as the angle containing a specified fraction of tracks originating about the incident source direction. Using the directional response simulation, validated with data as described above, we find that a better measure of the performance results from combining the axial spread with the head-tail assignment.

We construct the directionality metric as follows: suppose a background-free detector observes N candidate

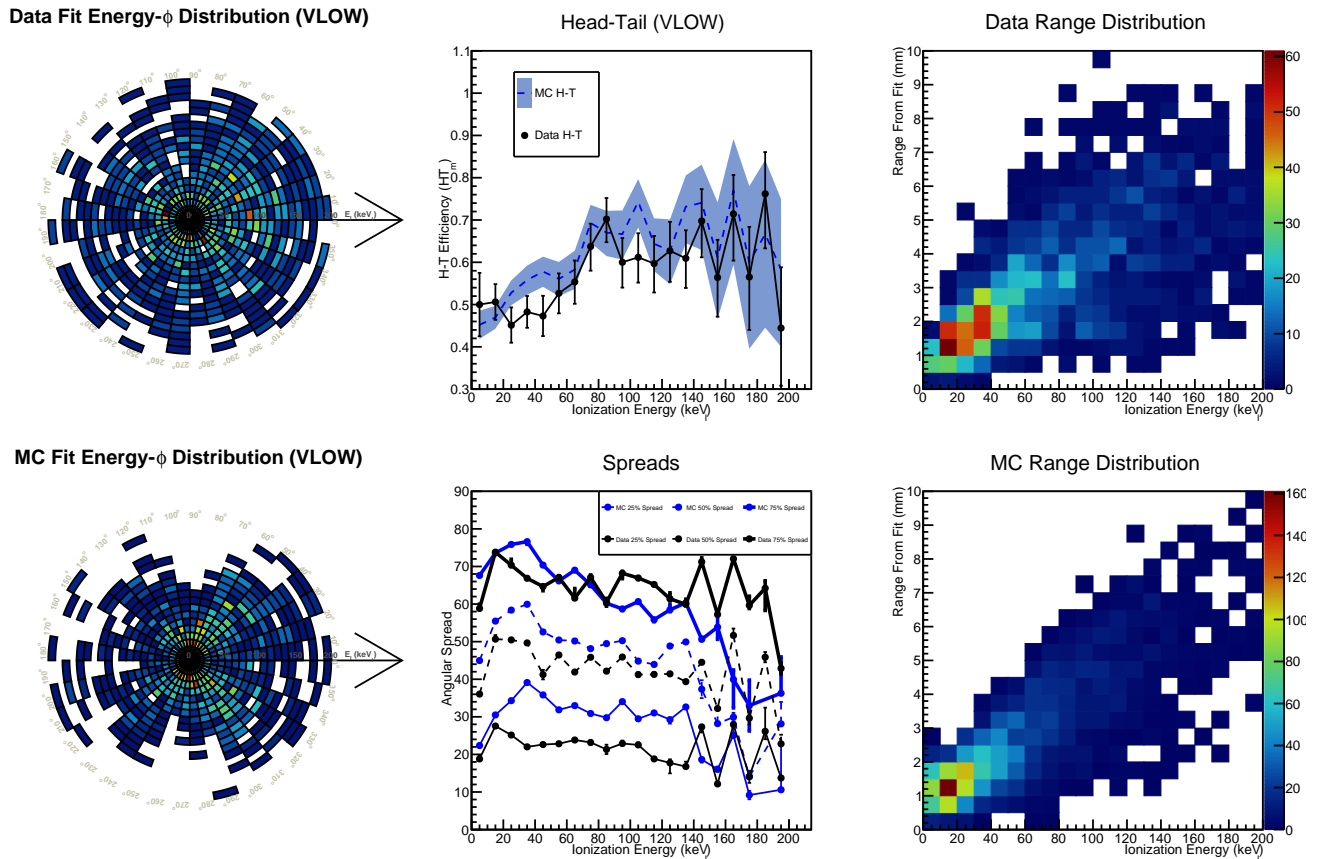


FIG. 6: Comparison of the directional response between data and simulation to a $d-d$ neutron generator using a test stand equipped with a cascaded triple-mesh amplification region. The simulation models the neutrons as monochromatic, although approximately 10% are expected to interact in the generator casing or chamber wall, possibly explaining the difference in axial response. The range-energy distributions (right) between the data and simulation are comparable. The colors on the energy- ϕ plots (left) scale linearly from ~ 0 (blue) to a maximum of 0.008 (red).

WIMP events, each with a reconstructed ionization energy and direction. For the set of recoils generated by those N interactions, we separate the directional response into head-tail and axial components and bin these variables in recoil energy, into bins of width ΔE_R . We compute the reconstructed forward fraction with respect to the expected WIMP direction, $HT(E_R)$, and the axial spread, $W(E_R)$. For a given energy bin of $HT(E_R)$ and $W(E_R)$, we calculate the probability that the observed value (or larger) could have arisen from an isotropic background distribution. We combine the p -values for each bin using Fisher's method [20] to create an overall isotropy rejection statistic.

For an isotropic background distribution, axial angles with respect to the expected WIMP axis are uniform between zero and ninety degrees. For the i^{th} energy bin containing a sample of m events, of which k events are along the expected WIMP axis, the probability of observing $HT > k/m$ is

$$p(HT > k/m) = I_{1/2}(k + 1/2, m - k + 1/2), \quad (2)$$

where $I_{1/2}$ is the regularized incomplete beta function [21], which is a continuum version of the binomial distribution. The subscript $1/2$ gives the probability of forward vs. backward scattering and the additional factors of $1/2$ in Eq. 2 are included in order to improve the coverage for a discrete distribution. For an isotropic background, the probability that half the tracks fall in a wedge of opening angle $\phi < W(E_r)$ around the expected WIMP axis is

$$p(\phi \leq W) = I_{W/90^\circ}([\!m/2\!] + 1, [\!m/2\!] + 2), \quad (3)$$

where $[\!m/2\!]$ is the floor of $m/2$. The subscript $W/90^\circ$ in Eq. 3 gives the probability for an event from an isotopic distribution for fall in an angle W around the WIMP axis. We compute the head-tail and axial probabilities p_i , as in Eqns. 2 and 3, for each energy bin, giving $2s$ degrees of freedom, where s is the total number of energy bins. We then combine the probabilities p_i into a χ^2 statistic,

$$\chi_{2s}^2 = -2 \sum_{i=0}^{2s} \log p_i. \quad (4)$$

We calculate the Fisherian p -value for rejection sensitivity, p_r , which is the probability that a measurement arises from the null (in this case isotropic distribution) hypothesis. This is the CDF of the χ_{2s}^2 distribution,

$$p_r = \frac{\gamma\left(s, -\sum_{i=0}^{2s} \log p_i\right)}{\Gamma(s)}. \quad (5)$$

where $\gamma(s, x)$ is the incomplete gamma function and $\Gamma(s)$ is the gamma function. In this way, we combine the head-tail statistic HT and spread statistic W for all energy bins.

We have verified that the resulting test statistic provides approximately uniform coverage for an isotropic input (i.e. a value of $p_r = 1\%$ occurs about 1% of the time), making it a valid metric for rejecting isotropy [8]. We do not claim to have developed the optimal test statistic, but instead focus on the main result of the paper, which is the performance of the metric on simulated WIMP recoil data, validated by the measurements described above. It is possible that a refined statistic could provide greater rejection power.

We now have the tools needed to quantify how well a directional detector can measure a directional signal for a given WIMP mass and rejection level p_r . We model a directional detector with a fiducial volume of one cubic meter and reconstruction performance as described in Section IV B, operating at a pressure of 30 torr and a gas gain of 100,000.

We start by generating 100 pseudo-experiments, each with N dark-matter-induced recoils ranging from $N = 50$ to 1,000 in increments of 50 events. The WIMP velocities are drawn from the three-dimensional Maxwell-Boltzmann distribution of the Standard Halo Model. We simulate two-body elastic scattering of WIMPs with mass $M_\chi = 10, 30, 100, 300$ and $1,000 \text{ GeV}/c^2$ off of ^{12}C or ^{19}F , with recoil kinetic energies above 25 keV, which is the approximate simulated track-detection threshold in the CCD. We model the full detector response and reconstruct the energy, axial direction, and head-tail assignment of each recoil track as described in Section III. Finally, we compute p_r from Eq. 5 for the ensemble of N recoils in each pseudo-experiment.

Fig. 7 shows the isotropy rejection for WIMPs with $M_\chi = 100$ and $1000 \text{ GeV}/c^2$, using HT or W only, and HT and W combined. For $M_\chi = 100 \text{ GeV}/c^2$, HT provides little rejection power, owing to limited intrinsic head-tail efficiency at low energies. HT becomes more powerful for $M_\chi = 1000 \text{ GeV}/c^2$ since the recoil energy spectrum is harder.

From the pseudo-experiments at each energy, we estimate the acceptance probability $p_a(N)$, or the fraction

of experiments achieving rejection probability p_r for a given number of signal events. We require $p_r = 0.001$, corresponding to 3σ rejection. The results for all simulated WIMP masses are shown in Fig. 8. For $M_\chi = 100$ (300) GeV/c^2 , 550 (450) events are required for rejection at the 3σ level in approximately half of the pseudo-experiments.

The number of required events can be reduced by selecting only those with reasonable directional reconstruction confidence. A head-tail assignment quality metric is derived from the fit used in reconstruction: after the initial fit, the fit is repeated forcing the opposite sense ΔS , and the likelihood ratio of the two senses is used to derive a head-tail quality metric. By cutting on the head-tail confidence such that the upper 50% of events are selected, we find that the number of required events to establish 3σ rejection of isotropy is reduced by 23% (17%) to 425 (375) total events (before the selection cut is applied) for $M_\chi = 100$ (300) GeV/c^2 .

We can now calculate the exposure (target mass \times live time) required for a detector to measure the number of events above a given energy threshold needed to reject isotropy at the level of $p_r = 0.1\%$. For this, we combine formulations from Ref. [7] (Eq. 3.9) and [22] (Eq. 1) to calculate the differential rate, dR/dE_R , of dark matter signal events as a function of recoil energy, E_R :

$$\frac{dR}{dE_R} = \frac{R_0}{E_0 r} \frac{1}{2\pi v_0^2} \int_{v_{\min}}^{\infty} \frac{d^3v}{v} f(\vec{v} + \vec{v}_E) \quad (6)$$

where

$$R_0 = \frac{490.43}{M_\chi M_T} \left(\frac{\sigma_0}{1 \text{ pb}} \right) \left(\frac{\rho_D}{0.39 \text{ GeV cm}^{-3}} \right) \left(\frac{v_0}{230 \text{ km s}^{-1}} \right) (\text{kg-day})^{-1}, \quad (7)$$

$$E_0 = \frac{1}{2} M_\chi v_0^2, \quad (8)$$

$$r = \frac{4M_\chi M_T}{(M_\chi + M_T)^2}, \quad (9)$$

$$\frac{v_{\min}}{c} = \frac{M_\chi + M_T}{M_\chi} \sqrt{\frac{E_R}{2M_T}}, \quad (10)$$

M_χ is the WIMP mass, $M_T = 0.932 A \text{ GeV}/c^2$ is the target mass, σ_0 is the WIMP-nucleus cross section for zero momentum transfer, ρ_D is the local dark matter density and \vec{v}_E is the Earth velocity relative to the dark matter distribution. $f(\vec{v})$ is the Maxwell-Boltzmann velocity distribution in the galactic frame, truncated at the galaxy escape velocity, v_{esc} , and v_0 is the dispersion velocity. An analytical expression for the integral in Eq. 6 is given in Appendix B of Ref. [22]. We use $\rho_D =$

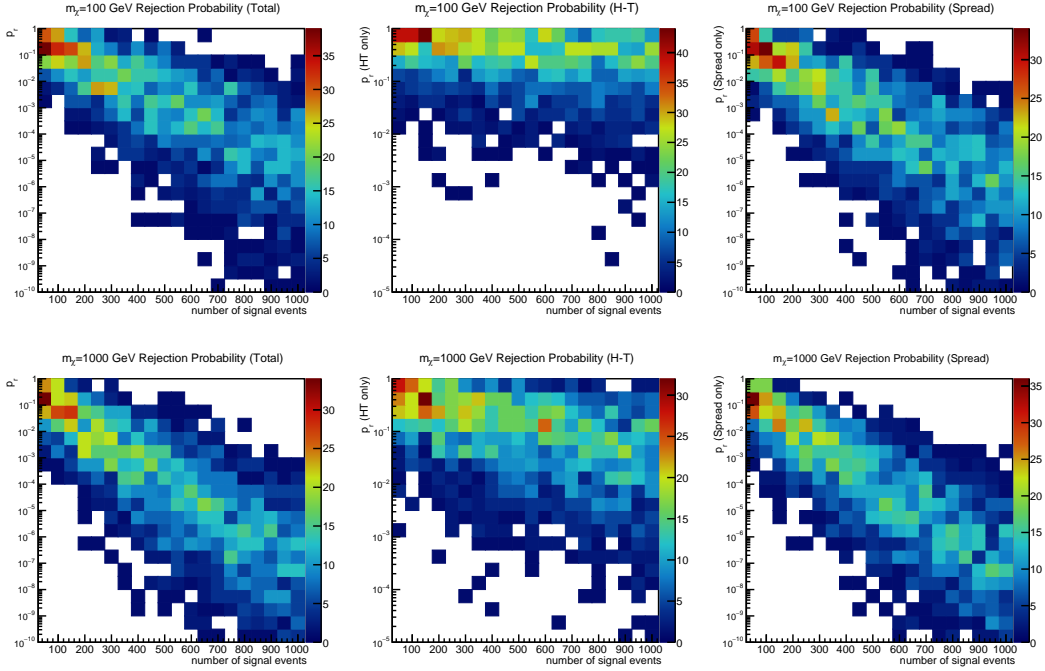


FIG. 7: Isotropy rejection (p_r) as a function of the number of signal events, N , for WIMPs with mass $M_\chi = 100 \text{ GeV}/c^2$ (top) and $1000 \text{ GeV}/c^2$ (bottom). The leftmost column shows the total rejection, the center column shows rejection from sense (head-tail) only, and the right column shows the contribution to rejection from the axial measurement. The color scale shows the percentage of pseudo-experiments for a fixed number of signal events.

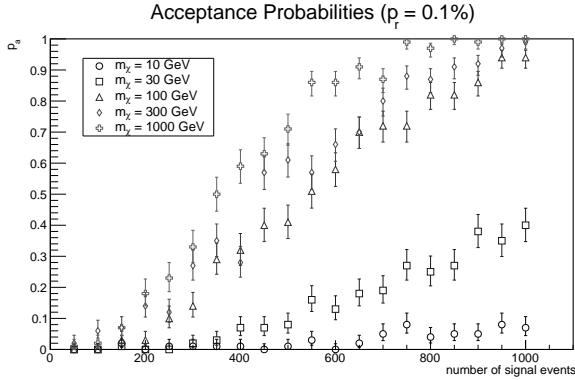


FIG. 8: The fraction of pseudoexperiments p_a achieving $p_r = 0.001$ for a given number of signal events N , for various simulated WIMP masses.

$0.39 \text{ GeV}/\text{cm}^3$ [23], $|\vec{v}_E| = 244 \text{ km/s}$, $v_{\text{esc}} = 544 \text{ km/s}$, and $v_0 = 230 \text{ km/s}$ here. To account for suppression of the cross section at large momentum transfer, we additionally include the spin-dependent form factor from Eq. 4.5 of Ref. [7].

Table I shows the number of cubic-meter-detector days required to detect one signal event for various WIMP masses, given a spin-dependent WIMP-fluorine cross section $\sigma_{0,F} = 1 \text{ pb}$ or a spin-dependent WIMP-proton cross section $\sigma_{0,p} = 1 \text{ fb}$. The equivalent values are

listed for a spin-dependent WIMP-proton cross section $\sigma_{0,p} = 0.49 \text{ fb}$, corresponding to the 95% upper limit predicted by a Constrained Minimal Supersymmetric Standard Model (CMSSM) [24] for $\mu > 0$, where μ is the Higgs/higgsino mass parameter. The detector performance demonstrated with the 4Shooter is assumed here, with an operating pressure of 30 torr of CF_4 gas and a fluorine target mass of 120 g. For WIMPs with mass 100 (300) GeV/c^2 and $\sigma_{0,F} = 1 \text{ pb}$, there will be one signal event, on average, every 62 (154) live days in a cubic-meter detector at the specified conditions and performance. Note that the rows corresponding to $\sigma_{0,p}$ require making standard spin-dependent assumptions [25] and include various spin factors, as well as the reduced mass of the WIMP-proton collision system.

The main result of this study is presented in Fig. 9, which shows the number of events needed to reject the isotropic hypothesis at 3σ for 50% of pseudo-experiments, as a function of WIMP mass, given a WIMP-fluorine cross section of 1 pb. This result accounts for the full directional response of the detector, from straggling of the primary ion, through reconstruction of the recoil track axis and head-tail assignment. For a WIMP mass of 100 (300) GeV/c^2 , 550 (450) events are needed to reject isotropy at the 3σ level half of the time. If a quality cut on the head-tail assignment is applied, only 425 (375) total events are needed, before selection. Using Table I, the latter case with head-tail quality cut translates to an exposure of 26,400 (57,800) cubic-meter-detector days.

M_χ (GeV/ c^2)	10	30	100	300	1,000
Percentage of recoils above 25 keV	0.038	15.5	37.8	45.9	48.8
Exposure per event (m ³ -days) for $\sigma_{0,F} = 1$ pb	6,678	46	62	154	481
Exposure per event (m ³ -days) for $\sigma_{0,p} = 1$ fb	147,063	364	272	541	1,563
Exposure per event (m ³ -days) for $\sigma_{0,p} = 0.49$ fb	300,129	743	554	1,105	3,191

TABLE I: Expected exposures (in cubic-meter-detector days) for various dark matter masses, given a spin-dependent WIMP-fluorine cross section ($\sigma_{0,F}$) of 1 pb or a spin-dependent WIMP-proton cross section ($\sigma_{0,p}$) of 1 fb or 0.49 fb [24]. An operating pressure of 30 torr of CF₄ gas and a fluorine target mass of 120 g have been assumed here.

This exposure is equivalent to an array of approximately 70 (160) cubic-meter detectors, or a single cubic detector with a fiducial length of 4.2 (5.4) m, operating for one year at 100% live time. Assuming a pressure of 30 torr CF₄, this corresponds to a fluorine target mass of 8.7 (19) kg. If the WIMP-proton cross section is 1 fb, the same array of detectors would require 4.4 (3.5) years at 100% live time to achieve the same sensitivity. This sets the scale for the experiment, using the current measured DMTPC detector performance.

The analogous statement for the current spin-independent cross section limits of 10^{-45} cm² requires 10^{11} cubic-meter-detector days, probably outside the limits of any low-pressure gas target detector.

Note that this discussion assumes perfect background rejection, i.e. that all recoils measured have been induced by WIMPs. While DMTPC has demonstrated excellent electron recoil rejection across a broad energy range [26], nuclear recoils from fast neutrons are indistinguishable on an event-by-event basis and will have approximately the same energy spectrum as that of elastic WIMP scattering, although these studies were carried out at a higher threshold. To study the effect of background on the sensitivity, an equal number of isotropically distributed nuclear recoil background events is added to the signal events, with the same energy spectrum as the signal. The result is shown in Fig. 9. As expected, the sensitivity is degraded by the presence of backgrounds: for a WIMP mass of 100 (300) GeV/ c^2 , 925 (750) events are needed to achieve the same sensitivity.

VI. OUTLOOK

This work has estimated the number of events required to reject isotropy in the distribution of candidate dark matter events using a full model of experimentally measured detector directional response for the first time. The model has been validated by detailed comparison with

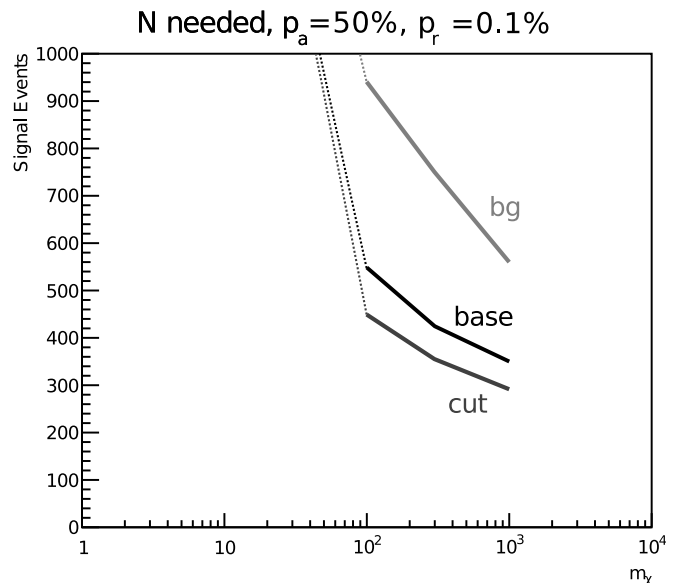


FIG. 9: Number of signal events required to reject the isotropic hypothesis at 3σ for 50% of pseudo-experiments, as a function of WIMP mass (M_χ), given a WIMP-fluorine cross section $\sigma_{0,F} = 1$ pb. The curve labeled “base” corresponds to Fig. 8, while the “cut” and “bg” curves show the effect of applying a quality cut on head-tail reconstruction or adding an equal number of isotropic background events as signal events, respectively. The number of events for the “cut” curve corresponds to the number of signal events before any cut is applied.

data of the reconstructed axial angle and head-tail assignment. Such a measurement would provide decisive evidence that a candidate dark matter signal is associated with the dark matter halo of our galaxy.

Improvements in sensitivity beyond the DMTPC detector performance presented here require improved head-tail efficiency at lower recoil energies. The model introduced here may be used to evaluate different de-

tector configurations. If the projected 2-D electrons at generator-level ‘truth’ are used to estimate the sense, rather than the corresponding reconstructed track, only 81 events are required to achieve the same sensitivity for a WIMP mass of $100 \text{ GeV}/c^2$. This gives an indication of the fundamental physics limit from ion straggling and shows that an alternative detector configuration, with e.g. a different gas target or medium, could provide up to a factor of five better sensitivity. Further improvements beyond this level would require targets with lower nuclear stopping at low energies, in order to reduce straggling of the primary ion and preserve more information about sense in the ionization distribution. Potential targets with lower mass sensitive to spin-dependent interactions are H and ^3He . The softer resultant recoil spectrum would likely require a higher gas gain in the amplification region, perhaps using the triple mesh in the cascaded configuration.

Alternatively, optimizing for axial direction reconstruction at increased operating pressure may be a sound strategy in light of the increasingly low limits on dark matter interaction cross sections. The model introduced here can be used to study the trade-offs between axial reconstruction performance, head-tail sensitivity, target type, and target mass.

In summary, for spin-dependent WIMP interactions, an array of 70–160 cubic-meter DMTPC detectors, or a single cubic fiducial volume measuring 4.2–5.4 m on one side (assuming that the effects from diffusion can be controlled), could make a decisive (3σ) determination at $\sigma_{0,p} \sim 1 \text{ fb}$ half of the time, with an exposure of approximately 4 live years, for WIMP masses between 100 and $300 \text{ GeV}/c^2$, assuming no background. There may be a factor of five improvement in performance with better targets and detector readout, but the energy straggling of the primary ion associated with the nuclear stopping power presents a significant barrier to further improvements in TPCs using gases such as CF_4 or CS_2 .

Appendix A: High-gain avalanches

Our 10 cm chamber is used to investigate operation at gains above 10^5 , Fig. 10. In the 10-cm chamber operating at a gain above 10^5 , we observe a peculiar feature of tracks associated to nuclear recoils: the tails of their transverse projection are non-Gaussian. Our simulation does not reproduce this feature. One explanation involves rare electron-impact processes producing states which can decay into ionizing ultraviolet photons. The UV photons travel up to 1 mm in the gas, larger than the

avalanche size, before ionizing, providing a mechanism for non-Gaussian track widths. Measurements in Ref. [27] indicate that there are processes at electron kinetic energies of 200 eV that produce UV photons. Inserting these rare processes into the simulation qualitatively produces long tails, but also results in a much higher gain since the photons travel in the direction opposite the electric field,

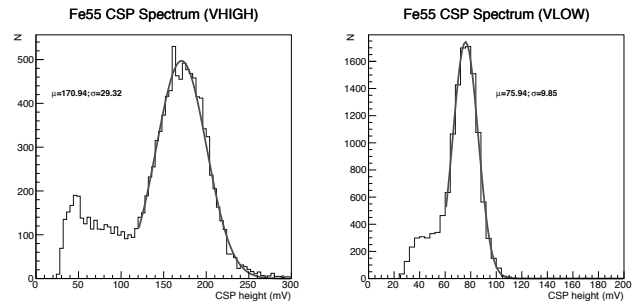


FIG. 10: Charge-sensitive preamplifier spectra of the 10 cm chamber with cascaded amplification regions at two different voltage settings with an ^{55}Fe source inside. Based on the 5.9 keV expected peak energy and preamplifier gain, the inferred gas gains are 437,000 and 984,000.

then ionize, creating a new avalanche. If this is indeed the mechanism responsible, there must also be some quenching that is not included in our model; `garfield++` does not include space charge effects, which could provide an explanation. Since the simulation does not reproduce the gain and spatial distribution simultaneously, the simulation was performed without the ionizing photons. The analysis of the data is therefore adjusted for the effective non-Gaussian convolution kernel by convolving with a sum of two Gaussians and adding two parameters (the second Gaussian width and ratio of amplitudes) to the fit. This shape matches the data well and could be motivated by the presence of two independent mean-free-paths (electron and UV photon).

Acknowledgments

This work was supported by NSF PHY-1004592, DOE de-sc0011970, STFC ST/K502261/1, ERC-2011-StG 279980, and the Royal Holloway University of London Crosslands Scholarship. We additionally thank Igal Jaegle for providing the `Geant4` simulation of the ISO spectrum moderated by a lead brick. Alex Leder provided valuable assistance with the *d-d* neutron generator.

-
- [1] D. Cline and M. Simpson (2015), 1504.04633.
 [2] S. Ahlen et al., *Int. J. Mod. Phys. A* **25**, 1 (2010).
 [3] J. B. Battat et al., *Nucl. Instrum. Meth. A* **755**, 6 (2014).
 [4] M. Leyton, *J. Phys.: Conf. Ser.* **718**, 042035 (2016).

- [5] D. Fancher et al., *Nucl. Instrum. Meth.* **161**, 383 (1979).
 [6] J. Ziegler, J. Biersack, and M. Ziegler, *SRIM - The stopping and ranging of ions in matter* (SRIM Co., 2008).
 [7] J. Lewin and P. Smith, *Astropart. Phys.* **6**, 87 (1996).

- [8] C. Deaconu, Ph.D. thesis, Massachusetts Institute of Technology (2015).
- [9] I. Wolfe, Bachelor's thesis, Massachusetts Institute of Technology (2010).
- [10] L. G. Christophorou, J. K. Olthoff, and M. Rao, *JPCRD* **25**, 1341 (1996).
- [11] A. Kaboth et al., *Nucl. Instrum. Meth.* **A592**, 63 (2008).
- [12] C. Geuzaine and J.-F. Remacle, *International Journal for Numerical Methods in Engineering* **79**, 1309 (2009), ISSN 1097-0207, URL <http://dx.doi.org/10.1002/nme.2579>.
- [13] C.-I. C. for Science, ELMERFEM, <http://elmerfem.org>.
- [14] H. Schindler and V. R., GARFIELD++, <http://garfieldpp.web.cern.ch/garfieldpp>.
- [15] F. James and M. Winkler, *MINUIT User Guide* (2004).
- [16] J. Lopez, Ph.D. thesis, Massachusetts Institute of Technology (2013).
- [17] O. Guillaudin et al., *EAS Publ. Ser.* **53**, 119 (2012), 1110.2042.
- [18] *ISO 8529-1: Reference neutron radiations – Part 1: Characteristics and methods of production* (2001).
- [19] S. Agostinelli et al., *NIM A* **A506**, 250 (2003), ISSN 0168-9002, URL <http://www.sciencedirect.com/science/article/pii/S0168900203013688>.
- [20] R. A. Fisher, *Statistical Methods for Research Workers* (Oliver and Boyd, 1925).
- [21] W. Eadie, D. Drijard, F. James, M. Roos, and B. Sadoulet, *Statistical Methods in Experimental Physics* (North-Holland, 1982).
- [22] C. McCabe, *Phys. Rev.* **D82**, 023530 (2010).
- [23] R. Catena and P. Ullio, *JCAP* **1008**, 004 (2010).
- [24] L. Roszkowski, R. Ruiz de Austri, and R. Trotta, *JHEP* **0707**, 075 (2007).
- [25] D. Tovey, R. Gaitskell, P. Gondolo, Y. Ramachers, and L. Roszkowski, *Phys. Lett.* **B488**, 17 (2000).
- [26] J. Lopez et al., *Nucl. Instr. Meth.* **A696**, 121 (2012).
- [27] S. Wang, J. Forand, and J. McConkey, *Can. J. Phys.* **67**, 699 (1989).